Combined SANS, SEC, NMR, and UV−Vis Studies of Simultaneous Living Anionic Copolymerization Process: Simultaneous Elucidation of Propagating Living Chains at Three Different Length Scales

Yue Zhao,[†] Hirokazu Tanaka,[†,‡,§] Nobuyoshi Miyamoto,[†,∥] Satoshi Koizumi,*[,†] and Takeji Hashimoto*[,†,‡]

Advanced Science Research Center (ASRC), Japan Atomic Energy Agency (JAEA), Tokai, Ibaraki 319-1195, Japan, Department of Polymer Chemistry, Graduate School of Engineering, Kyoto University, Katsura, Kyoto 615-8510, Japan

Received August 1, 2008; Revised Manuscript Received December 30, 2008

ABSTRACT: We studied a simultaneous living anionic copolymerization of styrene (S) and isoprene (I) monomers in a dilute solution with deuterated benzene as a solvent by means of combined time-resolved measurements of small-angle neutron scattering (SANS), size exclusion chromatography (SEC), nuclear magnetic resonance (NMR), and ultraviolet−visible spectroscopy (UV−vis). We observed structural change of the living chains during the polymerization process in three different length scales on the same solution and in a single batch, which enabled us to explore simultaneously the time changes in the local structure (living chain ends), the primary structure (propagating chains), and the higher order structure (the star-like local aggregates of the living chains). We found the copolymerization process is divided into two time regions, defined by regions I and II. In region I, the copolymerization of S and I monomers occurred and all I monomers were consumed at the end of region I, while in region II, pure polystyrene (PS) block chains are formed. In the beginning of region II (region II_a), living polymers having isoprenyl anion (PI^-) started to change rapidly into those having styryl anion (PS^-), and followed by a slow change from PI^- to PS^- in the latter part of region II (region II_b). As a consequence of the polymerization of S monomers under the coexistence of PI^- and PS^-, we found the following two phenomena: (i) an increase in M_w/M_n; (ii) the effective conversion rate of S monomers being slow compared with the corresponding homopolymerization of S monomers. The theoretical analysis of the time-resolved SANS profiles elucidated the time change in the association number of the living chain ends n: $n \sim 4$ in region I, n decreases from 4 to 2 in region II_a, and $n \sim 2$ in region II_b.

I. Introduction

In this paper, we aim to report our experimental studies of a simultaneous living anionic copolymerization of nondeuterated styrene (S) and isoprene (I) monomers in deuterated benzene (B-d_6) as a nonpolar solvent. For this study, we prescribed sufficiently low concentrations of S and I such that propagating copolymer chains are in a dilute solution throughout the copolymerization process, thereby never causing microphase separation contrary to our previous study.[1] This condition enables us to investigate time change in association number of living chain ends, n, throughout the copolymerization process, by means of a time-resolved (Tr-) small-angle neutron scattering (SANS) method. We employed a simultaneous measurement of Tr-SANS, SEC (size exclusion chromatography), NMR (nuclear magnetic resonance), and UV−vis spectroscopy for the same reaction solution in a single batch. Combining the four Tr-techniques, we are able to observe the structural change of living polymer chains in three different length scales on a rigorously common time scale, e.g., the changes in microscopic structural elements (i.e., the species at the living chain ends themselves), propagating primary structure (i.e., the molecular weight and its distribution of "arm" chains, and a sequence distribution of S and I along the "arm" chain), and a higher-order chain structure in mesoscopic scale (i.e., the "star-like local aggregates" of the living chains induced by the association of living chain ends), and interrelationships between these structural changes. The "arm chain" will be defined later in section IV. Here, the star-like aggregates are considered to be a lower level structure of the so-called giant worm-like micelles, if they exist. In this work, we have not aimed to explore the giant worm-like micelles, simply because the SANS q range, which was focused on the studies of the local aggregates and their smaller level structures, was not appropriate to permit the investigation of the giant micelles.

It is reported that the reactivities between living chain ends and monomers S or I are much different in a nonpolar solvent[2]

$$k_{SI} \gg k_{SS} > k_{II} > k_{IS} \quad (1)$$

where k_{AB} denotes the rate constant for propagation reaction from PA^- into PAB^-, with A and B being S or I. Because of this relationship, a growing polymer spontaneously changes from polyisoprenyl anions (PI^-) to polystyryl anions (PS^-) and vice versa during the copolymerization process.[2,3] The different reactivity ratio of S and I leads to the formation of so-called "tapered block copolymer chain",[4−8] which has a gradient of composition along the copolymer chain in either monomer: I is mainly polymerized first until its concentration becomes relatively low, whereas S starts incorporating in the propagating polymer chains with increasing amounts as the reaction continues, and after complete consumption of I, a pure PS block is formed.

It is also reported that in a nonpolar solvent the living chain ends tend to form association structures via electrostatic interactions of living chain ends.[9−14] By using a light scattering technique in living anionic polymerization of S to PS, Worsfold et al.[9] investigated the association behavior of living PS^-, whose

* To whom correspondence should be addressed.
[†] Advanced Science Research Center (ASRC), Japan Atomic Energy Agency.
[‡] Department of Polymer Chemistry, Graduate School of Engineering, Kyoto University.
[§] Present address: R&D Center, Mitsui Chemicals, Inc., 580-32 Nagaura, Sodegaura, Chiba 299-0265, Japan.
[∥] Present address: Department of Life, Environment, and Material Science, Faculty of Engineering, Fukuoka Institute of Technology, 811-0295 Fukuoka, Japan.

10.1021/ma8017519 CCC: $40.75
Published on Web 02/05/2009

living chain end is capped with isoprenyl lithium, in cyclohexane, which is a nonpolar and Θ-solvent for PS. They concluded that the association number of the living chain ends, n, ranges from 2.8 to 4.1 for PS with molecular weight of $(1.0-1.6) \times 10^5$. Recently the SANS technique emerges as a powerful tool for *in situ* observation of the living anionic polymerization process. Fetters, Richter, and co-workers[10] have reported that star-like aggregates with $n \sim 4.0$ are present during living anionic homopolymerization of I monomers in deuterated heptane. They suggested the presence of the giant worm-like aggregates also, which are higher order superstructures of the star-like local aggregates of the living chains, during living anionic homopolymerization of butadiene (B), S, or I in nonpolar solvents.[10−13]

The giant worm-like micelle itself is an intriguing large scale structure of the living polymers to be further studied as a function of the effective concentration of living ends and molecular weight of the living polymers not only for living homopolymerization but also for living sequential and simultaneous copolymerizations. In this work, however, we did not focus on exploration of the giant micelle as our primary objective. This is because roles of the giant micelles on reaction kinetics of the homopolymerization and copolymerization are not explicitly clear to us. It seems to us that the local aggregates of chain ends (*e.g.*, dimers or tetramers) are more directly related to the copolymerization reaction kinetics than their higher order couterparts, i.e., the giant micelles or aggregates. Hence we focus on simultaneous explorations of the local aggregates with the monomer conversions, species of the living chain ends, and molecular weight of the living polymers on the same batch of the copolymerization reaction solution.

Until now, there have been many studies concerning the association numbers of living chain ends in the living anionic homopolymerizations.[9−13] However, up to now there have been no studies which aim to investigate *in situ* (1) how the association number of chain ends varies during the simultaneous copolymerization process of S and I monomers, and (2) how the change affects the reaction itself, such as time changes in the molecular weight and the molecular weight distribution, the fraction of living-chain-end species (PS^- or PI^-), the monomer conversions, and the sequence distribution along the living chains.

In order to address the questions raised above, it is crucial to simultaneously investigate *in situ and at real time*, the changes in (i) association number, n, (ii) the primary structures of a single chain, including molecular weight, molecular weight distribution, the monomer conversions, and the sequence distribution of S and I along the copolymer chain, and (iii) chemical species of the living chain ends during the polymerization process *for the same reaction solution* in a single batch. We would like to stress that there have been no works reported so far along the line as described above. In the combined Tr-methods to be reported here, the Tr-SANS measurements are introduced to evaluate the time evolution of (i) n.[10−14] SEC and NMR measurements as a function of time are applied to yield information on time change in (ii) the primary structure. The Tr-UV−vis spectroscopy is used to estimate (iii) the fraction of PI^- or PS^- in the reaction solution with time.

It is worthy to note the merits of using SANS in this study as follows: (i) Because of the low energy of neutrons compared to X-ray, the polymerization reaction itself is not affected by the radiation of the neutron beam. (ii) High transmittance of neutrons enables us to observe the structures of living polymers in dilute solution in a quartz cell. (iii) By using nondeuterated S and I as monomers and deuterated benzene as a solvent, we can reasonably treat the SANS scattering from propagating copolymers chains as that from homopolymer chains, because the contrast for neutron between the two monomeric units is small relative to that between the monomeric units and deuterated solvent, as will be detailed in Supporting Information I. Owing to this fact, the time change in the association number, n, can be estimated on the basis of the scattering theory developed for the star-shaped homopolymers.[12,15]

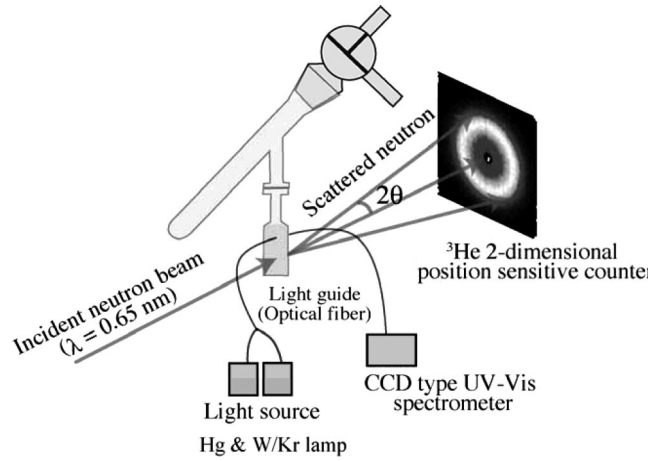

Figure 1. Schematic illustration of simultaneous *in situ* SANS measurement and UV−vis spectroscopy.

We like to note that this work is an extension of our previous preliminary work, which dealt with a simultaneous living anionic copolymerization reaction in such a concentrated solution that brought about the polymerization-induced self-assembly of block copolymers via disorder−order and order−order phase transitions.[1]

II. Experimental Section

II-1. Living Anionic Polymerization. First, a 90 μL solution of 1.0 M *sec*-butyllithum in cyclohexane and 6.3 mL of deuterated benzene were added into the specially designed reaction vessel (see Figure 1 and details to be described below). Then, a prescribed amount of I and S monomers (0.259 g or 0.38 mL and 0.263 g or 0.29 mL, respectively) was added into the vessel to start the polymerization, such that the initial weight ratio of S, I, and B-d_6 is 4:4:92. Thus the concentration of the polymer solution obtained at the end of the polymerization, C_{final}, is calculated to be 8 wt % from the compositions of the initial solution, which is sufficiently lower than the overlap concentration, C^* ($C_{final}/C^* \sim 0.5$).[16] Thus it is well expected that no microphase separations take place during the polymerization process. The reaction solution was kept at 25 °C.

In order to eliminate the contamination of the system with water and air during the polymerization, we designed a reaction vessel with two branches, as shown in Figure 2.[14] The reaction vessel is filled with dry argon gas and capped with a three-way stopcock. The living anionic polymerization is initiated in the vial tube of 20 mL (part A). The injection of reagents to the vessel and sampling up the solution for SEC and NMR measurements from the vessel are conducted from the top (part C), under the dry argon gas flowing from the side (part D). For SANS and UV−vis spectroscopy experiments, the solution is transferred into the quartz cell of 2 mm thickness (part B), which is connected to the vessel by a Teflon-coated O-ring.

The effective initiator concentration calculated was 10.6 mM, while the theoretical initiator concentration calculated was 12.7 mM.[17] This means that about 16% of the initiator was killed due to impurities brought about in the polymerization process in this work. We think the value is small enough so that the polymerization is well controlled.

II-2. SANS Measurement. The experimental procedure for Tr-SANS measurement is schematically illustrated in Figure 1.

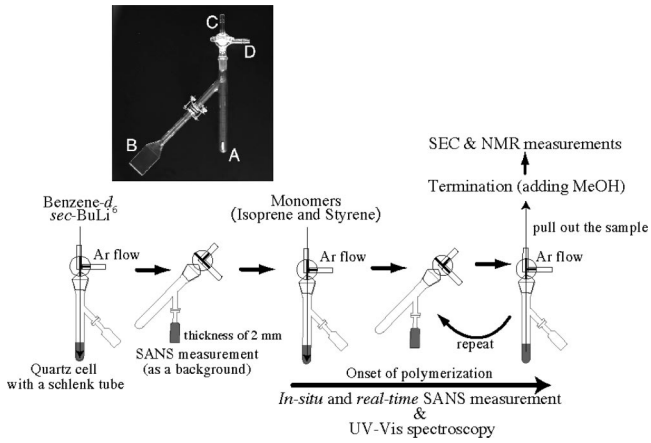

Figure 2. Experimental setup and procedure for simultaneous and time-resolved SEC, NMR, SANS, and UV−vis spectroscopy for the same reaction in a single batch.

Tr-SANS measurements were performed with SANS-J-II at research reactor JRR-3, JAEA, Tokai, Japan.[18] The incident neutron beam was monochromatized with a velocity selector to have the average wavelength (λ) of 6.5 Å with the wavelength distribution as characterized by $\Delta\lambda/\lambda = 12\%$. During the SANS measurements, the sample solution was controlled at 25 °C with an accuracy of ±0.5 °C. The scattered neutrons were detected with a two-dimensional ^{3}He position sensitive detector. The 2-dimensional scattering patterns were circularly averaged to obtain scattering profiles as a function of q, where q is a magnitude of the scattering vector, defined by $q = (4\pi/\lambda)\sin(\theta/2)$ with θ being the scattering angle. Thereafter, we consistently used Å as the unit of q. The obtained scattering profiles were corrected for background scattering, electronic noise of detector, detector sensitivity, and transmission, and finally normalized with a porous aluminum plate, which serves as a secondary standard, to give the absolute intensity scale (cm^{-1}).[18] The incoherent scattering intensity is small because B-d_6 comprises 92 wt % of the system. It was estimated to be ~0.11 cm^{-1} from the volume-averaged incoherent scattering intensity of B-d_6 and monomers I and S. The estimated incoherent scattering was subtracted from the observed net absolute scattering intensity.

II-3. SEC and NMR Measurements. As shown in Figure 2, we conducted SEC (Tosoh GPC-8220 with a refractive index detector) and NMR (proton NMR spectra were recorded at a Larmor Frequency of 400 MHz on a INOVA-plus, Varian Technologies, using a 5 mm high resolution triple resonance probe optimized for proton observation) measurements on aliquots taken at different reaction times. Prior to SEC and NMR measurements, the aliquots were first taken up from the reaction solution and terminated by adding a proper amount of deuterated methanol, both processes being conducted under the flow of the dry argon gas. Then tetrahydrofurane (THF) was used to dilute the solution to ~0.2 wt % for SEC measurements, and deuterated chloroform ($CDCl_3$) was used to make a ~0.5 wt % solution for NMR measurements.

II-4. UV−Vis Spectroscopy. We measured Tr-UV−vis spectroscopy simultaneously with SANS during polymerization process for the exactly same reaction solution. Figure 1 schematically shows *in situ*, *real-time*, and simultaneous SANS and UV−vis spectroscopy experiments.[14,19] Two kinds of light source were used for an incident UV−vis light. One is a mercury lamp with wavelength of 190 ~ 500 nm, and the other is a tungsten/krypton lamp with wavelength of 350−1700 nm. In this study, the wavelength is selected between 190 and 600 nm. The UV−vis spectra were collected with optical fibers and a CCD type detector (StellaNet, Inc., Tokyo, Japan) and corrected for background (quartz cell) spectrum.

Generally, the time (t) dependence of UV absorbance at a characteristic wavelength, $A(\lambda; t)$, reflects the time change in the concentration of the relevant component in the reaction system. According to the Lambert−Beer law,[20] $A(\lambda; t)$ at a given reaction time, t, is proportional to the concentration of the component X, [X(t)] (M), at the given t,

$$A(\lambda;t) = \varepsilon[\mathrm{X}(t)]l \tag{2}$$

where ε ($M^{-1}cm^{-1}$) is the absorption coefficient of component X, and l is the pass length (cm). Taking the absorbance at the end of the reaction, $A_\infty(\lambda)$, as a reference, one can obtain the fraction of X at a given time, $\phi_x(t)$, by calculating the relative extent of absorbance change, $A(\lambda; t)/A_\infty(\lambda)$, versus t

$$\phi_x(t) = A(\lambda;t)/A_\infty(\lambda) = [\mathrm{X}(t)]/[\mathrm{X}(t=\infty)] \tag{3}$$

where x is equal to PS^- in this particular case.

It is well-known that the absorption maximum of PI^- appears at $\lambda \sim 250$ nm,[21] and those of PS^- appear at both $\lambda \sim 350$ and $\lambda \sim 450$ nm.[22] Thus, by following $A(\lambda; t)$, we can estimate in principle the reduced concentration of both PI^- [$\phi_{PI}^-(t)$] and PS^- [$\phi_{PS}^-(t)$] as a function of t. However, benzene also shows broad peaks between 160 to 210 nm, which brings inaccuracy to the estimation of $\phi_{PI}^-(t)$. Moreover, the tail of the absorption maximum of PI^- contributes the absorption at ~350 nm as well, which makes the estimation of $\phi_{PS}^-(t)$ at 350 nm complicated. Above all, UV absorbance at $\lambda = 500$ nm, A(500 nm), a tail of the absorption maximum at ~ 450 nm, is selected to estimate $\phi_{PS}^-(t)$ in a following section, section III-2. Since [$PS^-(t=\infty)$] can be estimated from the molecular weight of the polymer at the end of the polymerization and the after termination, one can estimate [$PS^-(t)$] from the measured $\phi_{PS}^-(t)$. One can also evaluate [$PI^-(t)$] by using the relation [$PS^-(t)$] + [$PI^-(t)$] = [$PS^-(t=\infty)$].

III. Results

III-1. Time-Resolved SEC and NMR Measurements. Typical chromatograms obtained by the SEC measurements during the living polymerization process were demonstrated in Supporting Information II. The number-averaged molecular weight of the polymer at the end of the polymerization and after the termination, $M_{n,final}$, was calculated to be ~7000, from the corresponding apparent number-averaged molecular weight of the copolymer, $M_{n,app}$, calculated from the SEC measurements on the basis of PS standard. The correction to obtain $M_{n,final}$, from $M_{n,app}$ at the end of polymerization, and after the termination, $M_{n,final,app}$, is detailed in ref 23. M_n at a given t, $M_n(t)$, was also estimated from $M_{n,app}$ at the given t. The polydispersity index (PI) characterizing molecular weight distribution, M_w/M_n, is ~1.12 at the end of the polymerization and after the termination, where M_w denotes the weight-averaged molecular weight of the polymer.

Since both I and S monomeric units in the living polymer chains could be clearly identified by NMR spectroscopy (details can be found in Supporting Information III), one can estimate the monomer conversions for both I and S monomers as a function of time, which are defined as $C_I(t)$ and $C_S(t)$, respectively. Note that we deliberately chose spectra for polymers to calculate monomer conversions in order to avoid effects of evaporation of monomers during the sampling process.

Figure 3a shows the time dependence of $C_I(t)$ and $C_S(t)$. Their characteristic behaviors can be classified into two time regions, defined by region I and region II, as shown on the top of the figure and as separated by the vertical solid line. In region I ($0 \le t/\mathrm{min} \le 295$), $C_I(t)$ increases fast and reaches ~1.0 at the end of this region, whereas $C_S(t)$ increases slowly and reaches

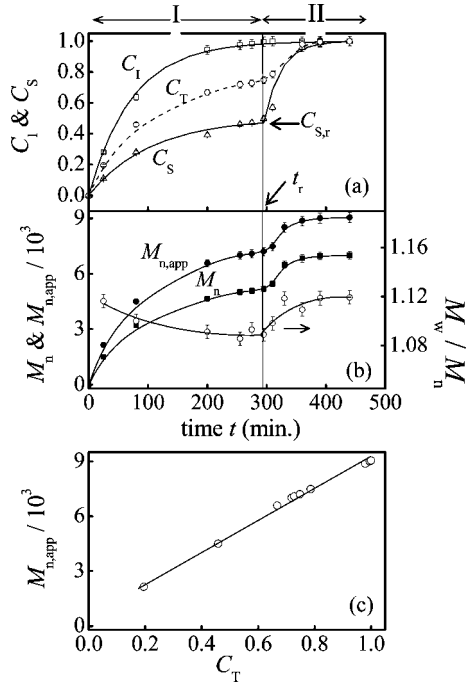

Figure 3. Time dependence of (a) monomer conversions, (b) $M_{n,app}$, M_w/M_n, and M_n, and (c) $M_{n,app}$ vs the total conversion, C_T, during the living anionic polymerization process. The vertical solid line indicates the time at the end of region I ($t \sim 295$ min.). The lines drawn for $M_{n,app}$ and M_w/M_n are only for visual guides, while that for C_I is given by eq 14, that for C_S is given by eq 15 for region I and by eq 16 for region II, that for C_T is given by eqs 4 and 14−16 and that for M_n is given by eq 4.

a steady value of 0.47 at the end of the region. In region II ($295 \leq t/\text{min} \leq 440$), only S monomers exist, and the consumption rate of S monomers in this region is much faster than that in region I. The broken line in Figure 3a represents the total conversion of I and S monomers, $C_T(t) \equiv [C_I(t) + C_S(t)]/2$, as a function of time, t. The result reveals a two-step increase of C_T with t. The characteristic time where C_I effectively reaches 1 is defined by t_r ($t_r \sim 295$ min), and $C_S(t)$ at t_r is defined by $C_{S,r}$ (=0.47), which will be utilized later in conjunction with Figure 11. Note that from pieces of information on $C_I(t)$, $C_S(t)$, $M_{n,final}$ and on the initial feeding ratio of both monomers (50:50 wt %), M_n at a given time, $M_n(t)$, can be determined by

$$M_n(t) = [C_I(t) + C_S(t)]M_{n,final}/2 = C_T(t)M_{n,final} \quad (4)$$

Here $M_{n,final}$ is given by ref 23, if the copolymerization proceeds according to a truly "living" polymerization.

Figure 3b shows time dependence of $M_{n,app}$ and M_w/M_n estimated from SEC measurements. The corrected value of M_n calculated from eq 4 is also shown as a reference. In region I, either $M_{n,app}$ or M_n increases rapidly at $0 \leq t/\text{min} \leq 200$, and then slowly at $200 \leq t/\text{min} \leq 295$ to an approximately steady value. In region II, $M_{n,app}$ or M_n starts again to increase rapidly with time at $295 \leq t/\text{min} \leq 330$, then followed by a slow increase to a final value. The observed two-step increase in $M_{n,app}$ or M_n with t is well consistent with the results previously reported for the simultaneous copolymerization.[24,25] As for M_w/M_n, in region I at $t = 30$ min, the earliest accessible reaction time in this study, M_w/M_n is ~1.12. As the copolymerization reaction proceeds, it gradually deceases to a constant value of 1.08, as expected. However, we find another increase in M_w/M_n from 1.08 to 1.12 in region II. Figure 3c shows that the $M_{n,app}(t)$ measured by SEC linearly increase with the $C_T(t)$ measured by NMR, indicating that the copolymerization follows the living polymerization. Hence it is natural that the change in

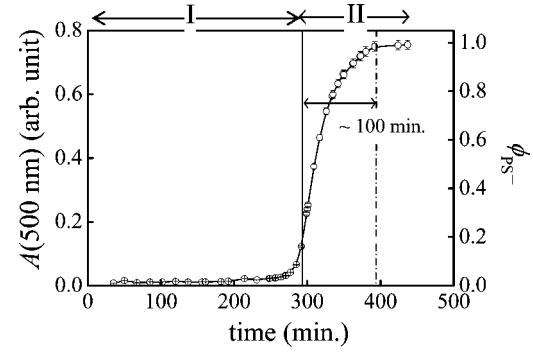

Figure 4. Time change in A(500 nm) (left ordinate axis) and ϕ_{PS}^- (right ordinate axis) during the whole polymerization process. The vertical solid line indicates the time at the end of region I ($t \sim 295$ min.), while the dash-dot line indicates the time where ϕ_{PS}^- reaches unity.

$M_{n,app}$ and C_T with t are identical, including the stepwise behavior.

III-2. Time-Resolved UV−Vis Spectroscopy. The solution before polymerization ($t = 0$), containing only *sec*-butyllithium and deuterated benzene, shows no absorption maximum in the wavelength range covered in this study. In region I, $A(\lambda = 350$ nm; $t)$ [defined hereafter A(350 nm) for simplicity] shows a slight increase with time, due to a small increase of [PS^-], as we mentioned in section II-4. At $t \geq 270$ min, A(350 nm) starts to increase remarkably with time, and we find an increase in $A(\lambda = 500$ nm; $t)$ [defined hereafter as A(500nm) for simplicity] also, due to the increase of [PS^-].The increase in A(500 nm) is accelerated in region II, and no change is found at $t \geq 400$ min. It is worthy to note that after termination, absorption maxima disappear and the spectrum shows similar to that for the solution before the polymerization. The details are given by ref 26.

Figure 4 shows the time change in A(500nm) during the polymerization process. In region I, A(500 nm) is very small and almost independent of time, except for a slight increase at the end of the region. In region II, it increases rapidly with time until $t \sim 400$ min, beyond which it shows almost a constant value, $A_\infty(500\text{ nm}) = 0.75$. Therefore ϕ_{PS}^- reaches unity, as shown in the right ordinate axis in Figure 4. The vertical dash-dot line is drawn at t ~ 400 min., where A(500 nm) reaches the steady value and ϕ_{PS}^- reaches unity. It is noted that [PS^-] and [PI^-] at a given time can be evaluated from $[PS^-] = \phi_{PS}^-(t)[PS^-(t = \infty)]$ and $[PI^-] = [\text{Ini}] - [PS^-] = [1 - \phi_{PS}^-(t)][\text{Ini}]$ noting that $[PS^-(t = \infty)] = [\text{Ini}]$, where [Ini] is the effective initiator concentration [10.6 mM] measured from $M_{n,final}$.

III-3. Time-Resolved SANS Measurement. Figure 5a shows Tr-SANS profiles at representative reaction times during the copolymerization process. In region I, the scattering cross section (intensity), $d\Omega/d\Sigma$, at all q range increases with time. However, in region II at $295 < t/\text{min} \leq 330$, $d\Omega/d\Sigma$ at $q < 0.05$ Å^{-1} decreases, while $d\Omega/d\Sigma$ at $q > 0.08$ Å^{-1} increases. After 330 min., $d\Omega/d\Sigma$ at all q range only slightly increases with time. Thus the time change in $d\Omega/d\Sigma$ depends on the q range.

In order to investigate the time change in SANS profiles more quantitatively, it is useful to select the average scattering at the low and high q ranges, which are designated by the two arrows labeled Q_L and Q_H in Figure 5a, to evaluate the respective average scattered intensity, defined by

$$Q_L \equiv \int_{q_{L1}}^{q_{L2}} \frac{d\Sigma}{d\Omega}(q)\, dq / \int_{q_{L1}}^{q_{L2}} dq \quad (5)$$

$$Q_H \equiv \int_{q_{H1}}^{q_{H2}} \frac{d\Sigma}{d\Omega}(q)\, dq / \int_{q_{H1}}^{q_{H2}} dq \quad (6)$$

where $q_{L1} = 0.017$ Å^{-1}, $q_{L2} = 0.032$ Å^{-1}, $q_{H1} = 0.10$ Å^{-1}, and $q_{H2} = 0.12$ Å^{-1}. The time change in Q_L and Q_H are presented

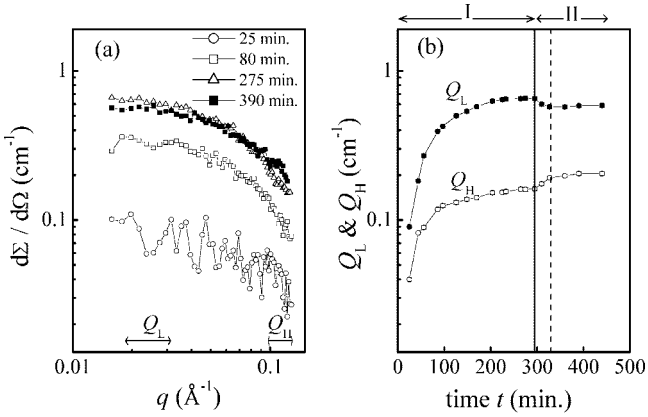

Figure 5. (a) Time evolution of SANS profiles at four representative reaction times ($t \sim 25$ min, 80 min, 275 min, and 390 min) during the copolymerization process. The SANS profiles were corrected for incoherent scattering. (b) Time dependence of Q_L and Q_H during the copolymerization process, where Q_L and Q_H are the average scattering intensity in the low and high q regions indicated by arrows in part a. The vertical solid line and broken line indicate the time at the end of region I ($t \sim 295$ min), and at $t \sim 330$ min, respectively.

in Figure 5b. In region I, both Q_L and Q_H first increase rapidly with time and then slowly reach nearly constant values in the end of the region. However, in the beginning of region II at $295 \leq t/\text{min} \leq 330$, Q_L decreases with time, but at $t \geq 330$ min., Q_L starts to again increase only slightly. The vertical broken line indicates $t = 330$ min., beyond which Q_L starts to increase. This trend will be discussed later in conjunction with Figure 8 in section IV-3.

Unlike Q_L, Q_H keeps increasing with t in both regions I and II and increases stepwisely in the boundary between the two regions, as M_n or C_s does (Figure 3). On the basis of Q_L and Q_H, we can obtain a clear-cut, *direct experimental prediction concerning the time change in n* of living chains during the copolymerization process for the following reasons. Q_L and Q_H reflect the structural change of living polymer chains in the large and small length scales, respectively. Namely, Q_L depends primarily on the associating structures composed of the multiple living polymer chains as a whole, while Q_H depends almost on the single living polymer chain, i.e., the M_w after the termination. The increase in Q_H in the beginning of region II suggests that M_w of a single polymer chain (an arm chain) undergoes the second-step increase in this time region. If the association structure of the multiple chains does not change across the boundary between regions I and II, Q_L also is expected to undergo the second-step increase in region II as Q_H does. On the contrary, the decrease in Q_L against this expectation thus reveals itself the decrease of the association number in the multiple living polymer chains in the beginning of region II.

III-4. SANS Profiles before and after the Termination Reaction. Figure 6a and 6b demonstrate comparisons of the SANS profiles before and after the termination of the living polymers at $t = 200$ min in region I and $t = 440$ min at the end of region II, respectively. The profiles shown by squares and circles in both figures indicate the profiles for the living polymer and the terminated polymer, respectively. Upon termination, $d\Omega/d\Sigma$ at $q < 0.08$ Å^{-1} decreases significantly, whereas it does not change much at $q > 0.1$ Å^{-1}. The decrease in $d\Omega/d\Sigma$ at low q suggests disappearance of the association structures upon termination, which is in turn due to the electrostatic neutralization of the chain ends after the termination. The solid lines in the figure will be discussed in the next section. The trend observed upon termination is consistent with the earlier reports.[10−12,14]

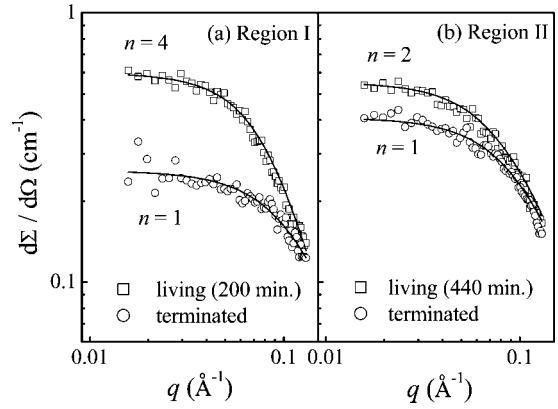

Figure 6. Comparison of the SANS profiles before (squares) and after (circles) termination in (a) region I at 200 min and (b) region II at 440 min. The solid lines show the best-fitted theoretical scattering curves.

IV. Theoretical Analysis of SANS Profiles

IV-1. Scattering Theory. We aim to quantitatively analyze the Tr- SANS profiles in order to evaluate time change in n. For this purpose we assumed that: (i) the copolymer in B-d_6 can be approximated by homopolymer having an average coherent scattering cross section of monomeric units of S and I; (ii) the aggregated living copolymers can be approximated by an n-armed star-shape homopolymer, where n stands for the association number, as in the earlier works by Fetters, Richter and co-workers.[10−13]

The scattering function (differential scattering cross-section) for dilute solutions of the n-arm star polymers at a given time t during the polymerization is given by

$$d\Sigma/d\Omega(q;t) = \frac{b_v(t)^2}{N_A} \frac{\phi(t)[1-\phi(t)]}{\frac{1}{\rho(t)M_{w,star}(t)P_{star}(q;t)} + 2A_2(t)\phi(t)} \quad (7)$$

where $b_v(t)$ is the scattering contrast discussed in detail in Supporting Information IV, N_A is Avogadro's number, and $\phi(t)$ is the volume fraction of the polymers in the solution. The quantities $M_{w,star}(t)$, $\rho(t)$,$P_{star}(q;t)$ and $A_2(t)$ are the weight average molecular weight, the density, the form factor, and the second virial coefficient of the star polymer, respectively. Note that eq 7 is obtained from the well-known equation for the coherent scattering from a dilute solution at polymer concentration C (g/mL),

$$\frac{KC}{d\Sigma/d\Omega(q)} = \frac{1}{M_w P(q)} + 2A_2C + \ldots \quad (8)$$

where $K = b_v(t)^2/N_A$, $C \equiv \rho(t)\phi(t)$, and $\phi(1-\phi) \sim \phi$ at low polymer concentrations. M_w and $P(q)$ in eq 8, which are the weight average molecular weight and the form factor of polymers, respectively, correspond to $M_{w,star}(t)$ and $P_{star}(q;t)$ in eq 7.

As in the earlier works,[12,13] we assume $P_{star}(q;t)$ is given by Benoit's form factor for the Gaussian n-arm star chains

$$P_{star}(q;t) = \frac{2}{n(t)x^2}\left\{(x-1) + \exp(-x) + \frac{n(t)-1}{2}[1-\exp(-x)]^2\right\} \quad (9)$$

where $x \equiv q^2R_g(t)^2$, and $R_g(t)$ is the radius of gyration of the Gaussian arm polymer chain. Validity of the assumption (i) made in the beginning of this section is discussed in detail in Supporting Information I.

IV-2. Evaluation of Characteristic Parameters. In eq 7, $M_{w,arm}(t)$ is given by $M_{w,arm}(t) = PI(t)M_n(t)$, where $PI(t)$ and $M_n(t)$

are the polydispersity index and number average molecular weight of the arm polymer at a given time t, respectively. Both $PI(t)$ and $M_n(t)$ can be determined from the SEC and NMR data for the solution terminated at the given time t. Moreover, $M_n(t)$ is given by eq 4, where $M_{n,final}$ in turn is evaluated as detailed in ref 23. The quantities $\phi(t)$, $b_v(t)$, and $\rho(t)$ in eq 7 can be evaluated also from the experimental results as described in detail in Supporting Information IV. Since eq 9 assumes the Gaussian star polymer chains, we calculated $R_g(t)$ in eq. 9 on the basis of the same assumption, which gives $R_g(t) = [N(t)a^2/6]^{1/2}$, where $N(t)$ is the total number of monomeric units per arm chain at a given time $[N(t) = N_{S,final}C_S(t) + N_{I,final}C_S(t)]$, with $N_{X,final}$ (X = S and I) being the total number of monomeric unit of X per arm chain at the end of the polymerization as detailed in ref 23. a is the averaged segment length ($a = 0.68$ nm).[27,28]

From eq. 7 we can obtain for dilute star-shaped polymers,

$$KC\left[\frac{1}{d\Sigma/d\Omega(q)} - \frac{1}{d\Sigma/d\Omega(q=0)}\right] = \frac{1}{M_{w,star}}\left[\frac{1}{P_{star}(q)} - 1\right] \quad (10a)$$

We can experimentally evaluate the function in the left-hand side of eq 10a and compare it with the theoretical function by using $P_{star}(q)$ given by eq 9 where $n(t)$ is the only unknown parameter, because $R_g(t)$ can be experimentally determined as described above. The best-fit between the experimental and theoretical functions yield $n(t)$. Then $A_2(t)$ can be estimated from

$$A_2(t) = \frac{1}{2C(t)}\left[\frac{KC(t)}{d\Sigma/d\Omega(q=0;t)} - \frac{1}{M_{w,star}(t)}\right] \quad (10b)$$

by noting $M_{w,star} = n(t)M_{w,arm}$ where $M_{w,arm}$ can be experimentally determined. Practically, $d\Sigma/d\Omega(q = 0; t)$ can be estimated from the extrapolations of the scattered intensity at lower q region to $q = 0$ by using Guinier's approximation,[29,30]

$$d\Sigma/d\Omega(q;t) = d\Sigma/d\Omega(q=0;t)\exp[-q^2R_{g,star}(t)^2/3] \quad (11)$$

In eq 11, $R_{g,star}(t)$ denotes the radius of gyration of the star polymer at a given t. The details of the Guiniers plot and evaluated $R_{g,star}(t)$ will be found in Supporting Information V. For simplicity, we ignore polydispersity in $n(t)$ but we allow noninteger values for $n(t)$.

IV-3. Results of Theoretical Analysis. The solid lines in Figure 6a and Figure 6b show the theoretical scattering curves best-fitted with the experimental scattering profiles obtained before and after the termination reaction in the two time regions I and II, respectively. In each figure, the two solid lines are obtained by using the same R_g for the arm polymer chain but different n values. The best-fitted theoretical curves for the experimental profiles before the termination reveal that n is 4 in Figure 6a but n is 2 in Figure 6b. After the termination, we found that $n = 1$ in both cases as reasonably expected for the neutral chain ends, consistent with earlier reports.[10−12,14] The evaluated n values in the current copolymerization process agree well with the literature values for the homopolymerization, where n is ∼4 for PI^-,[9−12,14] and n is ∼2 for PS^-.[9−12]

Figure 7 shows the best-fit of some representative experimental scattering profiles (shown by the symbols) with the theoretical profiles (shown by the solid lines) using $n(t)$ as the only adjustable parameter. The scattering profile 1 obtained at the earliest time covered in this experiment has a relatively weak scattered intensity, especially at high $q \sim 0.1$ Å^{-1} so that the evaluation of n at this time is suffered from a relatively large error. Thus obtained $n(t)$ values are shown in Figure 8 as a function of time. The results are summarized as follows: (i) In region I, $n(t)$ shows a constant value of approximately equal to 4. (ii) At the early stage of region II ($295 \le t/\text{min} \le 330$), defined hereafter as region II_a, $n(t)$ tends to rapidly decrease with time from 4 to 2, though the theoretical analysis was not applied to this region, simply because the association number of the living chain ends may have a distribution between $n = 2$ and 4, and the given analysis is based on no distribution on the value $n(t)$. (iii) At the late stage of region II ($330 \le t/\text{min} \le 440$), defined hereafter as region II_b, $n(t)$ shows an almost constant value of 2.

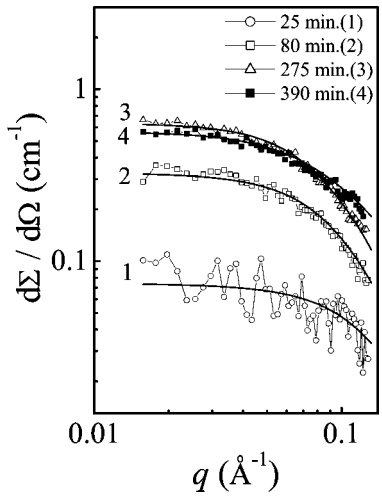

Figure 7. Comparisons of experimental scattering profiles (symbols) and the best-fitted theoretical scattering curves (solid lines) at four representative reaction times ($t \sim 25$ min, 80 min, 275 min, and 390 min) during the copolymerization process.

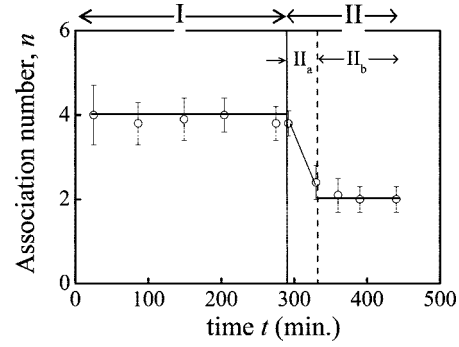

Figure 8. Time dependence of the association number n of the living chain ends. The vertical solid line indicates the time at the end of region I ($t \sim 295$ min), while the broken line indicates the time beyond which n is approximately equal to 2.

Since we evaluated both $M_n(t)$ (Figure 3) and $n(t)$ (Figure 8), we can plot $n(t)$ as a function of molecular weight (though not shown in this paper). We obtained a constant value of $n = 4$ for the range of M_n from ∼2000 to ∼5200 in region I, then n decreases from 4 to 2 in region II_a, and $n = 2$ when M_n exceeds 6500 in region II_b. According to the analysis of n as a function of molecular weight in the homopolymerization process of I or S in benzene, n asymptotically decreases from some large values to 4 (for PI) or 2 (for PS) with increasing M_n up to ∼2000.[12,31] In the time domain covered in Figure 8, M_n is larger than this critical molecular weight, so that we do not expect the molecular weight dependence of n in the reaction solution, and hence the change of n with M_n in region II_a reflects the change of n intrinsic to the change in the living chain ends from PI^- to PS^-.

V. Discussion

V-1. Sequence Distribution of I and S Monomers in Propagating (Tapered Block) Copolymer Chains. It is known that the different reactivity ratios of S and I results in the formation of a tapered block copolymer.[4−8] The sequence distribution of I and S monomers along the tapered block chain affects its morphology[32−34] and physical properties.[32−36] The clarification

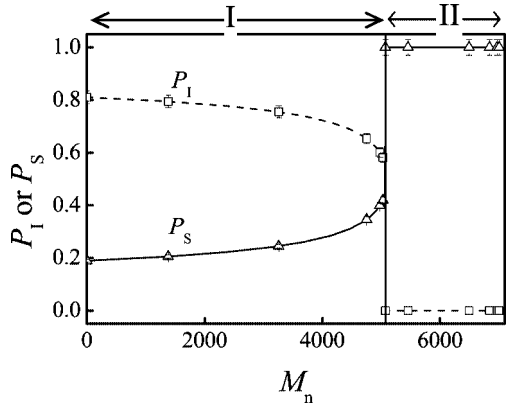

Figure 9. Average number fraction of I and S monomers (P_I and P_S, respectively) incorporated in a propagating copolymer chain as a function of M_n. The vertical solid line indicates the end of region I.

of the sequence distribution simultaneously with other parameters is indispensable for deep insights into not only the copolymerization process, as will be discussed in the next section, but also physical properties of the copolymers. In our study, owning to the knowledge of $C_I(t)$ and $C_S(t)$, we are able to determine the sequence distribution along the copolymer chain during the whole polymerization process. The detailed methods of the determination will be found in Supporting Information VI.

In Figure 9, the average number fractions of I (P_I) and S (P_S) monomers incorporated along the propagating copolymer chain are plotted as a function of M_n. The vertical solid line indicates the boundary between regions I and II. In region I, the decrease in P_I and the increase in P_S were found as follows: (i) in the early stage of the copolymerization of $M_n < 2000$, the polymer chain formed is close to the random copolymer with $P_I \sim 0.8$ and $P_S \sim 0.2$; (ii) when $2000 < M_n < 4500$, the part of chain formed has a small gradient of composition in either of the monomers, where P_I decreases from 0.8 to 0.7 and P_S increases from 0.2 to 0.3; (iii) when $4500 < M_n < 5200$ in the end of region I, a sharp gradient of composition in either of the monomers was observed, where P_I decreases from 0.7 to 0 and P_S increases from 0.3 to 1. In region II, $P_I \sim 0$ and $P_S \sim 1$, due to the absence of I monomers in the reaction solution. Therefore, pure PS block chains are formed in region II in the reaction solution.

V-2. Simultaneous Copolymerization Process and Mechanism As Observed by the Combined Time-Resolved Studies of Various Quantities Displayed on a Rigorously Common Time Axis. In this section we discuss in detail the simultaneous copolymerization process and mechanism in three length scales: (i) mesoscopic structure of multiple chain associations at the chain ends in terms of Q_L and n as observed by Tr-SANS, (ii) the primary structure of the single chains in terms of M_n and M_w/M_n, C_I or C_S, and P_I or P_S as observed by SEC and NMR, and (iii) microscopic structure of the chain ends in terms of ϕ_{PS^-} as observed by Tr-UV−vis. Comparisons of the time changes in all the parameters mentioned above on the common time scale are indispensable to gain deep understandings of the copolymerization process and mechanism, and thus they are shown together in Figure 10a−e without regard for redundancies.

Region I ($0 \le t/min \le 295$). C_I continuously increases with time up to 1.0, but C_S and M_n increase to an almost the constant values of 0.47 and 5200, respectively. P_I is always larger than P_S, indicating that the incorporation of I into the propagating chain outweighs the incorporation of S, as predicted by eq 1 and consistent with the previous reports.[3] M_w/M_n decreases with time from 1.12 to an almost constant value of 1.08. ϕ_{PS^-} is very small in this region except for the end of this region, indicating that almost all the living chain ends are expected to be composed

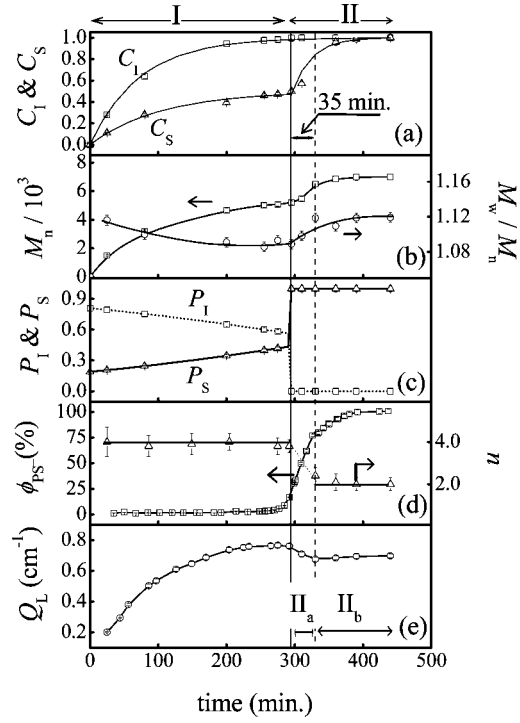

Figure 10. Summary of time dependence of the characteristic parameters plotted on the common time scale. (a) C_I and C_S, (b) M_n and M_w/M_n, (c) P_I and P_S, (d) n and ϕ_{PS^-}, and (e) Q_L. The vertical solid line and broken line indicate the time at the end of region I ($t \sim 295$ min) and region II_a ($t \sim 330$ min), respectively.

of PI^- and that the lifetime of PS^- is very short, reflecting the large value of k_{SI}. At the end of this region, $\phi_{PS^-} = 0.2$, $C_I = 1.0$, and $C_S = 0.47$. The result apparently means that 80% and 20% of the total living ends are occupied by PI^- and PS^- when 100% of I monomers and 47% of S monomers are consumed at the end of this region. These results may be theoretically explained on the basis of kinetic data k_{AB} (A, B = S or I) for the copolymerization kinetics, $n(t)$, and the effective initiator concentration. For this purpose, we need to further measure k_{AB} under our experimental condition, which deserves further works. The increase in Q_L observed in this time region reflects the increase in the size of the associating structures due to the increasing M_n of the single living chain under the fixed value of $n = 4$.

In region I, the following four propagation reactions occur:[3]

(i)

$$PI^- + I \rightarrow PI^-, \quad \text{with } -d[I]/dt = k_{II}[PI^-][I] = R_{II}[I], \quad \text{where } R_{II} \equiv k_{II}[PI^-] \quad (12a)$$

(ii)

$$PI^- + S \rightarrow PS^-, \quad \text{with } -d[S]/dt = k_{IS}[PI^-][S] = R_{IS}[S], \quad \text{where } R_{IS} \equiv k_{IS}[PI^-] \quad (12b)$$

(iii)

$$PS^- + I \rightarrow PI^-, \quad \text{with } -d[I]/dt = k_{SI}[PS^-][I] = R_{SI}[I], \quad \text{where } R_{SI} \equiv k_{SI}[PS^-] \quad (12c)$$

(iv)

$$PS^- + S \rightarrow PS^-, \quad \text{with } -d[S]/dt = k_{SS}[PS^-][S] = R_{SS}[S], \quad \text{where } R_{SS} \equiv k_{SS}[PS^-] \quad (12d)$$

where k_{AB} and R_{AB} are the rate constant ($M^{-1}s^{-1}$) and the apparent rate constant (s^{-1}), respectively, for addition of B

monomer into PA^-, giving rise to PAB^-. [X] (X = I, S, PI^- and PS^-) denotes the concentration of X. The total consumption rate or reaction rate of I, $-d[I]/dt$, is related with reactions i and iii by:

$$-d[I]/dt = R_I[I], \quad \text{where } R_I = R_{II} + R_{SI} = k_{II}[PI^-] + k_{SI}[PS^-] = k_{II}K_I^{1/4}[(PI^-)_4]^{1/4} + k_{SI}K_S^{1/2}[(PS^-)_2]^{1/2} \quad (13a)$$

where K_I is the equilibrium constant of polyisoprenyl anion between tetramers and unimers, and K_S is the equilibrium constant of polystyryl anion between dimers and unimers;

$$(PI^-)_4 \rightleftharpoons 4PI^-, \quad K_I = [PI^-]^4/[(PI^-)_4] \text{ and } (PS^-)_2 \rightleftharpoons 2PS^-, \quad K_S = [PS^-]^2/[(PS^-)_2] \quad (13b)$$

Here $(PI^-)_4$ and $(PS^-)_2$ designate the tetramer of PI^- and the dimer of PS^-, respectively, and $[(PI^-)_4]$ and $[(PS^-)_2]$ designate the concentration of $(PI^-)_4$ and $(PS^-)_2$, respectively.

It is generally accepted that the homopolymerization of S or I initiated with *sec*-BuLi in nonpolar solvent follows the first-order kinetics.[37] The first-order kinetics was also found to approximately fit well to C_I in this copolymerization experiment as well, as shown by the good agreement between the experimental values (symbols) and the solid line in Figure 3a, where C_I is given by:

$$C_I = 1 - \exp(-R_I t); \quad R_I = (2.25 + 0.11) \times 10^{-4}\ s^{-1} \quad (14)$$

In order to validate the first-order approximation, R_I in eq 13a should be a constant, independent of time. Actually, ϕ_{PS}^- in region I is almost a constant, which implies $[PI^-]$ and $[PS^-]$ and hence R_I are almost constants with time. This is why the first-order approximation works well for this copolymerization reaction. The same argument is applied to C_S, where C_S is given by

$$C_S/C_{S,r} = 1 - \exp(-R_S t); \quad R_S = (1.60 \pm 0.14) \times 10^{-4}\ s^{-1} \quad (15)$$

Moreover, R_I obtained from eq 14 is very close to the value, $R_{I,homo}$, for the homopolymerization of I [$R_{I,homo} = (2.27 \pm 0.11) \times 10^{-4}\ s^{-1}$] for the same total living chain concentration, the same solvent, and the same reaction temperature.[38] This result indicates the contribution of the second term $k_{SI}[PS^-]$ in eq 13a is really small, due to the very short lifetime of PS^- as a consequence of the large k_{SI} value.

Region II$_a$ (295 < t/min ≤ 330). Q_L starts to decrease from 0.75 to 0.7 with t, revealing qualitatively a decrease of n. P_I is always 0, while P_S is 1. The theoretical analysis described in section IV further shows that n decreases from 4 to 2. Concurrently ϕ_{PS}^- estimated from UV absorption at 500 nm (see eq 3) starts to rapidly increase from ~ 20% to ~ 80%. This rapid change in the living chain end from PI^- to PS^- is obviously due to the reaction of the living chain ends only with S monomers which remain in the system. The reaction with S only is believed to be the main cause for the decrease of n also. It may appear to be surprising at a first glance that it takes ~35 min for the living chain ends to deaggregate from tetramers to dimers. However, this is easily understood with the information obtained from $\phi_{PS}^-(t)$ obtained from the UV absorption as described above.

C_S, M_n, and M_w/M_n stepwisely increase in this region, due to the propagation of pure PS blocks. However, it is striking to note that a large fraction of PI^- ($\phi_{PI}^- \sim 20\%$) still survive even in the end of region II_a and in the early stage of region II_b, where I monomers are completely consumed. The surviving PI^- may possibly forms (i) the aggregates with $n = 4$, and (ii) mixed aggregates with n between 4 and 2, and these aggregates coexist with the PS^- aggregates with $n = 2$ at the end of region II_a. Some consequences of this fact will be presented in sections V-3 and V-4. In this case, the apparent value of n as determined by SANS is expected to be a noninteger value slightly larger than 2. The experimental results on n are consistent with this expectation, as the values for n slightly larger than 2 are well expected to be within the experimental errors.

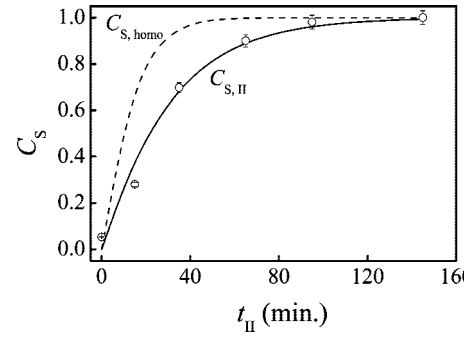

Figure 11. Comparison of monomer conversions of S in region II of our system (solid line) and that in the homopolymerization system (broken line) under the same polymerization conditions specified in the text.

Region II$_b$ (330 < t/min ≤ 440). C_S, M_n, and Q_L slightly increase with t, whereas ϕ_{PS}^- reaches its maximum (100%), and M_w/M_n reaches a constant value of 1.12. In this region, as well as in region II_a, only the polymerization of S to PS block chains takes place, as evidenced by $P_I \sim 0$ or $P_S \sim 1$.

V-3. Comparison between the Rate of Block Copolymerization of Styrene in Region II and the Rate of Homopolymerization of S. Since, in region II, only S monomers exist in the reacting solution, we expect the polymerization of pure S monomers to pure PS block chains under the influence of the PI^- living chain ends. Therefore, it is worthy to compare the polymerization rate of S to the PS block and the homopolymerization of S to homo PS under the same reaction conditions, such as the temperature (25 °C), solvent (B-d_6), and concentration of living chains (10.6 mM). This is because the comparison will clarify the effects of transformation of the chain-end aggregates from $(PI^-)_n$ to $(PS^-)_m$ on the reaction rate of S into PS^-. In order to do so, we should first separate the contribution of C_S in region II from that in region I for the copolymerization by introducing reduced monomer conversion of styrene in region II, $C_{S,II}$, defined by $C_{S,II} = (C_S - C_{S,r})/(1 - C_{S,r})$, and reduced time, t_{II}, defined by $t_{II} = t - t_r$, where $C_{S,r}$ and t_r have been already defined in Figure 3. Then, we plot $C_{S,II}$ vs t_{II} in Figure 11. Once again we note that t_r is the time at which all I monomers are effectively consumed.

The time dependence of monomer conversion of S in the homopolymerization, $C_{S,homo}$, is also shown with the broken line in Figure 11, as a reference.[38] The first-order kinetics approximation works well for both the copolymerization and homopolymerization, which is characterized by

$$C_{S,II} = 1 - \exp(-R_{S,II} t_{II}); \quad R_{S,II} = (5.83 \pm 0.8) \times 10^{-4}\ s^{-1} \quad (16)$$

as shown by the solid line and by

$$C_{S,home} = 1 - \exp(-R_{S,homo} t); \quad R_{S,homo} = (1.7 \pm 0.2) \times 10^{-3}\ s^{-1} \quad (17)$$

as shown by the broken line. A much slower reaction rate in the copolymerization system than that in the homopolymerization is found, except the very late stage of the reaction, i.e., $t_{II} \geq 100$ min, which is corresponding to $t \geq 400$ min. In other

words, $R_{S,II}$ is smaller than $R_{S,homo}$ by ~3 times. The suppression of the reaction rate may be due to a long life of PI^- living chain ends in region II, which may keep the chain end associations. ϕ_{PS}^- is found to just reach 100% at $t \geq 400$ min as shown in Figures 4 and 10d, indicating that PI^- are coexisting together with PS^- for a long time up to ~ 100 min after the complete consumption of I monomers. The long life of $[PI^-]$ in region II is expected to suppress the reaction rate of S, because it reduces concentration of $[PS^-]$ compared to $[PS^-]$ in the corresponding homopolymerization and because it involves the slow reaction (ii) in eq 12b with the small rate constant k_{IS}, which in turn may reflect a strong association strength of PI^- chain ends relative to that of PS^- chain ends.

V-4. Interpretation of Observed Increase in M_w/M_n in Region II. We like to give some comments on the observed increase in M_w/M_n in region II as shown in Figures 3b and 10b. As we discussed in section V-3, PI^- and PS^- coexist together in region II up to $t \sim 400$ min during the period of which PI^- slowly decays to zero concentration. In this time span, there may be a slow equilibration among dimers $(PS^-)_2$, tetramers $(PI^-)_4$, and mixed aggregates $(PI^-/PS^-)_x$ $(2 \leq x \leq 4)$. The living chains having PS^- ends in the dimers will propagate fast, while the living chains having PS^- ends in the mixed aggregates will propagate slowly. The existence of living chains having PI^- ends in the tetramers and/or the mixed aggregates, as revealed by $(1 - \phi_{PS}^-)$, simply means that these chains are not propagating. This offers the primary cause for the increase in M_w/M_n in this region. If the system had more S monomers than this experiment so that PS block chain could keep propagating at $t \geq 400$ min in region II, the effect of the PI^- survival in region II becomes less important, and M_w/M_n should tend to decrease with t to a constant value ~1.08.

V-5. Interpretation of Observed Slowing down of Growth Rate of M_n at the End of Region I. Here we would like to review that the slowing down of the rate of increasing M_n observed in the end of region I is quite naturally expected from eqs 1 and 12a. As we described earlier, ϕ_{PS}^- increases up to 20% in the end of region I. Therefore PI^- and PS^- coexist in the reaction solution, though most of the living chain ends are composed of PI^-. In the end of region I, $-d[I]/dt$ is small, simply because [I] is very small, which slows down the increase of C_I with t. $-d[S]/dt$ is also small, because k_{IS} is the least of the four rate constants, and because $[PS^-]$ is small in this time region. All these small possible propagation reaction rates lead to the observed slowing down of the growth rate of M_n in the end of region I.

VI. Concluding Remarks

The living anionic copolymerization of a mixture of isoprene (I) and styrene (S) monomers, in the dilute solution with deuterated benzene as a nonpolar solvent and *sec*-butyllithium as an initiator, was investigated by a simultaneous measurement of time-resolved small-angle neutron scattering (SANS), size exclusion chromatography (SEC), nuclear magnetic resonance (NMR), and ultraviolet−visible (UV−vis) spectroscopy. The combined time-resolved study on the same single batch reaction solution enabled us to investigate the structural change of the propagating living chains in three different length scales on a rigorously common time scale: living chain ends as shown by the parameter ϕ_{PS}^-, primary structure of single living chains as shown by the parameters M_n, M_w/M_n, C_I, C_S, P_I, and P_S, and the association of living chains as shown by the parameter n. Although the living anionic copolymerization of S and I has been studied extensively in the past, there is no study so far that uses such a combination of real-time methods as this study on the same single batch reaction solution.

All the experimental findings as described in the discussion section V may nicely agree with the "expected" behavior. However, the "expected behavior", which has been left without experimental proofs so far, was directly verified unequivocally by means of this unique experimental method. The reported change in the association number of the living chain ends during the copolymerization process also may be as "expected", but we could provide the first direct evidence that; it actually happens; when it starts; how long it lasts. The results imply the followings. The PI^- ends seemingly has a large association strength relative to the PS^- ends. As a consequence, the PI^- ends survive for a long time [~35 min for the decrease of $\phi_{PI}^- \equiv (1 - \phi_{PS}^-)$ down to 0.2 or ~100 min for the decrease of ϕ_{PI}^- down to ~0], even after a full consumption of I monomers. We propose that during this time span, there will be a slow equilibration among tetramers $(PI^-)_4$, mixed aggregates $(PI^-/PS^-)_x$ $(2 \leq x \leq 4)$ and dimers $(PS^-)_2$ and this equilibration results in the increase of M_w/M_n in region II and the slow reaction rate, $R_{S,II}$, of S monomers to pure PS blocks relative to the reaction rate, $R_{S,homo}$, of S monomers to homo PS, $R_{S,II} \sim (1/3)R_{S,homo}$.

In this work we have developed a methodology to extract simultaneously, in situ and at real time, the various fundamental quantities during the course of the living anionic copolymerization process on a *given reacting solution*. This methodology, which has been applied so far only to a few systems including living anionic homopolymerizations[14,31] and controlled radical polymerizations,[39,40] may be worthy being applied to many other samples in future. We are particularly interested in collaborations with researchers in this field.

It is intriguing to note that the time-change in the microscopic structure as observed in the time-change in the living chain ends affects the higher-order hierarchical structure levels of the living chains, such as the primary chemical structure (the molecular weight, its distribution and sequence distribution) and associating structures of the living chain ends. This offers a primitive example of information transmittance among different hierarchical structure levels, which are important in living biological systems in general.

Acknowledgment. This work was partly supported by a Grant-in-Aid (No. 17750114) for Young Scientists from the Ministry of Education, Culture, Sports, Science and Technology, Japan.

Supporting Information Available: Supporting Information I, determination of relative fluctuations of the coherent scattering cross-section along the copolymer chain; Supporting Information II, typical SEC chromatograms with Figure S1; Supporting Information III, NMR spectra to determine C_I and C_S with Figure S2; Supporting Information IV, determination of characteristic parameters required for calculating the theoretical SANS profiles with Table S1; Supporting Information V, Guinier plots and evaluation of $R_{g,star}$ with Figure S3 and Table S2; Supporting Information VI, determination of sequence distribution of the propagating copolymer chain from $C_I(t)$ and $C_S(t)$. This material is available free of charge via the Internet at http://pubs.acs.org.

References and Notes

(1) Yamauchi, K.; Hasegawa, H.; Tanaka, H.; Motokawa, R.; Koizumi, S.; Hashimoto, T. *Macromolecules* **2006**, *39*, 4531–4539.
(2) Szwarc, M.; Van Beylen, M. *Ionic polymerization and living polymers* Chapman & Hall: New York, 1993.
(3) Worsfold, D. J. *J. Polym. Sci. Part A* **1967**, *5*, 2783–2789.
(4) Zelinski, R. P. U.S. Patent 2975160, **1961**.
(5) Kraus, G.; Childers, C. W.; Gruver, J. T. *J. Appl. Polym. Sci.* **1967**, *11*, 1581–1591.
(6) Kraus, G.; Rollmann, K. W. *Angew. Makromol. Chem.* **1971**, *16/17*, 271–296.

(7) Hsieh, H. L. In *Block and Graft Copolymers* Burke, J. J., Weiss, V., Eds.; Syracuse University Press: Syracuse, NY, 1973.
(8) Aggarwal, S. L.; Livigni, R. A.; Marker, L. F.; Dudek, J. J. In *Block and Graft Copolymers* Burke, J. J., Weiss, V., Eds.; Syracuse University Press: Syracuse, NY, 1973.
(9) Worsfold, D. J.; Bywater, S. *Macromolecules* **1972**, *5*, 393–397.
(10) Stellbrink, J.; Allgaier, J.; Willner, L.; Richter, D.; Slawecki, T.; Fetters, L. J. *Polymer* **2002**, *43*, 7101–7109.
(11) Fetters, L. J.; Balsara, N. P.; Huang, J. S.; Jeon, H. S.; Almdal, K.; Lin, M. Y. *Macromolecules* **1995**, *28*, 4996–5005.
(12) Stellbrink, J.; Willner, L.; Richter, D.; Lindner, P.; Fetters, L. J.; Huang, J. S *Macromolecules* **1998**, *31*, 4189–4197. *Macromolecules* **1999**, *32*, 5321−5329.
(13) Niu, A. Z.; Stellbrink, J.; Allgaier, J.; Willner, L.; Radulescu, A.; Richter, D.; Koenig, B. W.; May, R. P.; Fetters, L. J *J. Chem. Phys.* **2005**, *122*, 134906.
(14) Miyamoto, N.; Yamauchi, K.; Hasegawa, H.; Hashimoto, T.; Koizumi, S. *Physica B* **2006**, *385*, 752–755.
(15) Benoit, H. *J. Polym. Sci.* **1953**, *11*, 507–510.
(16) The overlap concentration of the solution, C^* (g/cm^3), is defined as $C^*(R_{g,final}{}^3 4\pi/3) = M_{n,final}/N_A$, where N_A is Avogadro's number, $R_{g,final} \sim 2.5$ nm and $M_{n,\ final} \sim 7000$ are the radius of gyration and the molecular weight of one copolymer chain at the end of the polymerization and after the termination, respectively. Detailed calculations of $R_{g,final}$ and $M_{n,\ final}$ will be found in eq 9 and ref 23.
(17) Because some amount of initiators always become inactive due to the presence of impurities, in this study we calculated the effective initiator concentration and compared it with the fed initiator concentration in order to check if the polymerization process is well controlled or not. The effective initiator concentration is calculated as $[Ini]_{eff} = W_{ini}/M_{n,final} = 10.6$ mM, where W_{ini} represents the total weight of fed monomers (0.522 g) per total volume of the reaction system, $V_{total} = (90 \times 10^{-6} + 6.3 \times 10^{-3} + 0.38\times 10^{-3} + 0.29\times 10^{-3})\text{L} = 7.06 \times 10^{-3}$ L (74 g/L) before the polymerization, and $M_{n,final}$ represents the total molecular weight after the polymerization and termination (∼7000), as will be detailed in ref 23. The theoretical initiator concentration, $[Ini]_{theor}$, can be calculated from the fed initiator amount as $[Ini]_{theor} = n_{ini}/V_{total} \sim 12.7$ mM, where n_{ini} is moles of the fed initiator (90 μL solution of 1.0 M *sec*-BuLi).
(18) Koizumi, S.; Iwase, H.; Suzuki, J.; Oku, T.; Motokawa, R.; Sasao, H.; Tanaka, H.; Yamaguchi, D.; Shimizu, H. M.; Hashimoto, T *J. Appl. Crystallogr.* **2007**, *40*, s474−s479.
(19) Miyamoto, N.; Inoue, Y.; Koizumi, S.; Hashimoto, T *J. Appl. Crystallogr.* **2007**, *40*, s568−s572.
(20) Ingle, J. D. J.; Crouch, S. R. *Spectrochemical Analysis* Prentice Hall: Englewood Cliffs, NJ, 1988.
(21) Roovers, J. E. L.; Bywater, S. *Polymer* **1973**, *14*, 594–596.
(22) Stearne, J.; Smid, J.; Szwarc, M. *Trans Faraday Soc.* **1964**, *60*, 2054–2061.
(23) From SEC, the "apparent" number averaged molecular weight of the copolymer chain, $M_{n,app}$, can be calculated directly on the basis of polystyrene standard calibration. However, we must take into account the size difference between I and S monomeric units in the copolymer to estimate true molecular weight M_n from $M_{n,app}$. For this purpose, we used a calibration factor 1.6 estimated for homoPI. This factor 1.6 was determined by measuring $M_{n,PI,app}$'s by SEC with PS standard for a series of PI homopolymers having different $M_{n,PI}$'s which were independently measured by a membrane osmometer. We assume that the factor 1.6 is applicable to the copolymer also. We further assume that the "apparent" number average molecular weight per copolymer chain at the end of polymerization, $M_{n,final,app}$ (∼9000), can be expressed as follows:

$$M_{n,final,app} = 1.6M_I N_{I,final} + M_S N_{S,final} \sim 9000 \quad \text{(I)}$$

where M_X (X = I or S) is the molecular weight of X monomeric unit, and $N_{X,final}$ (X = I or S) is the number of X monomeric unit per chain at the end of the polymerization and after the termination of the living polymer. It should be noted that there is no theory that supports this assumption. On the other hand, there is no better way to handle the problem of determining molecular weight of the copolymers. Hence we use this assumption to obtain an approximate values for $M_{n,final}$. Since the initial monomer feeding ratio is known as 50:50 wt %, therefore,

$$M_I N_{I,final} = M_S N_{S,final} \quad \text{(II)}$$

From eqs I and II, $N_{I,final} = 51$, $N_{S,final} = 34$. The true number-average molecular weight of the copolymer at the end of the polymerization and after the termination, $M_{n,final}$, is therefore given by

$$M_{n,final} = M_I N_{I,final} + M_S N_{S,final} \sim 7000 \quad \text{(III)}$$

(24) Tanaka, Y.; Sato, H.; Nakafutami, Y.; Kashiwazaki, Y. *Macromolecules* **1983**, *16*, 1925–1928.
(25) Korotkov, A. A.; Rakova, G. V. *Vysokomol. Soedin.* **1961**, *10*, 1482–1490.
(26) Tanaka, H. *Ph.D. Dissertation* . Department of Polymer Chemistry, Graduate School of Engineering, Kyoto University: Kyoto, Japan, 2008.
(27) Ballard, D. G. H.; Wignall, G. D.; Schelten, *J. Eur. Polym. J.* **1973**, *9*, 965–969.
(28) Petychakis, L.; Floudas, G.; Fleischer, G. *Europhys. Lett.* **1997**, *40*, 685–690.
(29) Guinier, A.; Fournet, G. *Small-Angle Scattering of X-rays*; Wiley: New York, 1955.
(30) Roe, R. J. *Methods of X-ray and Neutron Scattering in Polymer Science*; Oxford University Press: New York, 2000.
(31) Miyamoto, N.; Koizumi, S.; Hashimoto, T. Manuscript in preparation.
(32) Tsukahara, Y.; Nakamura, N.; Hashimoto, T.; Kawai, H.; Nagaya, T.; Sugimura, Y.; Tsuge, S. *Polym. J.* **1980**, *12*, 455–466.
(33) Hashimoto, T.; Tsukahara, Y.; Kawai, H. *Polym. J.* **1983**, *15*, 699–711.
(34) Hashimoto, T.; Tsukahara, Y.; Tachi, K.; Kawai, H. *Macromolecules* **1983**, *16*, 648–657.
(35) Hodrokoukes, P.; Floudas, G.; Pispas, S.; Hadjichristidis, N. *Macromolecules* **2001**, *34*, 650–657.
(36) Hodrokoukes, P.; Pispas, S.; Hadjichristidis, N. *Macromolecules* **2002**, *35*, 834–840.
(37) Hsieh, H. L. *J. Polym. Sci. Part A* **1965**, *3*, 153–161.
(38) The homopolymerization rates of I, $R_{I,homo}$, as a function of [PI$^-$] and those of S, $R_{S,homo}$, as a function of [PS$^-$] in benzene at 25 °C were determined by Miyamoto et al.[31]

$$\log R_{I,homo} \cong 0.25 \times \log[PI^-] - 3.15 \quad \text{(IV)}$$

$$\log R_{S,homo} \cong 0.4 \times \log[PS^-] - 1.98 \quad \text{(V)}$$

where the units for $R_{X,homo}$ and [PX$^-$] (X = I or S) are s^{-1} and M, respectively. According to these two equations, $R_{I,homo} = 2.27 \times 10^{-4}$ s^{-1}, $R_{S,homo} = 1.7 \times 10^{-3}$ s^{-1} at the anion concentration of [PX$^-$] = 10.6 mM, which is the same total anion concentration as the copolymerization reaction in this study.
(39) Motokawa, R.; Iida, Y.; Zhao, Y.; Hashimoto, T.; Koizumi, S. *Polym. J.* **2007**, *39*, 1312–1318.
(40) Motokawa, R.; Koizumi, S.; Zhao, Y.; Hashimoto, T. *J. Appl. Crystallogr.* **2007**, *40*, S645−S649.

MA8017519